Simulation of high-energy ion collisions with graphene fragments

Sergiy Bubin,[1] Bin Wang,[1] Sokrates Pantelides,[1,2,3] and Kálmán Varga[1]
[1]*Department of Physics and Astronomy, Vanderbilt University, Nashville, Tennessee 37235, USA*
[2]*Department of Electrical Engineering and Computer Science, Vanderbilt University, Nashville, Tennessee, 37235, USA*
[3]*Oak Ridge National Laboratory, Oak Ridge, Tennessee 37830, USA*
(Received 30 April 2012; published 19 June 2012)

The collision of energetic ions and graphene fragments is studied in the framework of real-space finite-difference time-dependent density functional theory (TDDFT) coupled with classical molecular dynamics for nuclei. The amount of energy transferred from the projectile to the target is calculated to explore the defect formation mechanisms as a function of the projectile's energy. It is found that creation of defects in graphene due to the interaction of a fast proton with valence electrons is unlikely. In the case of projectiles with higher charges, the transferred energy increases significantly, leading to higher probability of bond breaking.

DOI: 10.1103/PhysRevB.85.235435 PACS number(s): 61.80.Jh, 34.50.Bw, 81.07.Bc

I. INTRODUCTION

Graphene[1,2] is considered to be a very promising material in various applications. By patterning graphene in different ways, nanoribbons, and quantum dots can be created. Focused ion beams is one of the most promising approaches for etching and patterning graphene.[3–7] While the interaction of particle radiation and solids has long been studied experimentally and theoretically,[8–14] their effect on single-layer materials is expected to be very different from that of bulk materials.[15] The study of radiation is also valuable for graphene-based electronics and sensors to be used in outer space and low earth orbit, where a significant exposure to energetic ions may occur.

Ion irradiation can be used to introduce structural defects in graphene and other carbon allotropes,[16] and provides a versatile tool for manipulating their physical properties.[7,17–22] For this purpose, proton irradiation, in particular, attracts much interest due to the observed irradiation-induced magnetism in graphite and graphene,[23–29] which was attributed to defects, e.g., vacancies and H species.[24] However, an atomic-resolved determination, e.g., through high-resolution transmission electron microscopy, of the defects that are generated by proton irradiation has not been achieved, indicating the need for research to answer this open question and for controllable introduction of defects to achieve enhanced magnetism.

To simulate high-energy ions such as protons impinging on graphene, the electronic excitations in the ion-collision process have to be taken into account. It has been shown that for a high-energy H atom impacting onto graphene, the results of time-dependent density functional theory (TDDFT)[30] differ significantly from the Born-Oppenheimer approximation due to the growing role of electronic excitations[31] above H impact energy of 400 eV. These simulations suggest that the total energy transfer to the target increases with increasing proton energy, but these studies were limited to an energy range up to 10 keV.[31] It is still unclear whether defects can be generated at a higher proton energy. Moreover, to mimic proton irradiation in various experiments[23,28,29] where fast H^+ ions with kinetic energy ranging from a few hundred kilo-electron-volt to a few mega-electron-volt were used, it would be very valuable to extend the simulations to that energy range and also explore the effect of the charge state of the projectile.

In this paper, using time-dependent density functional theory combined with molecular dynamics simulations, we simulate the trajectory-dependent interaction of small graphene fragments with high-energy ions (proton and $^4He^{2+}$) with energies up to 2 MeV. The energy transferred to the target reaches the maximum, about 65 eV, at proton energy of around 30 keV, with most of the energy transfer accumulated in electronic excitations. More energy is transferred to the target when the projectile passes through a C-C bond than the center of the carbon ring due to the higher electron density located at the bonds. In the whole energy range, we have not observed any bonds broken except by head-on collision. However, by using a more positively charged α particle, $^4He^{2+}$, the maximum total-energy transfer is about 150 eV, much higher than that of using proton. For the smallest fragment of graphene used in the calculation, a benzene molecule, the C-C bond was broken when the 50 keV particle goes through the bond, indicating that the mechanism of radiation effect on graphene may be different for highly charged ions.

II. METHOD

TDDFT has been successfully used in various time-dependent quantum mechanical simulations, e.g., in nonperturbative calculations of properties of systems in intense laser fields[32–34] or to study the scattering of energetic atoms with carbon nanostructures.[31,35,36]

In the present simulations, a high-energy ion hits the graphene sheet at preselected positions. The high-energy ion is represented by a moving Coulomb field, that is, we neglect the effect of the target on the motion of the projectile. This assumption is reasonable in the high-energy ranges that we are studying. The TDDFT simulation of the electronic density is supplemented by an Ehrenfest-type molecular dynamics for the nuclear motion. This approach allows us to monitor the motion of atoms and to measure the energy deposited in the target as a function of the energy of the projectile. The advantage of this approach is that both the electronic and nuclear motion are treated simultaneously and it is possible to track and visualize coupled electron-ion dynamics.

Various computational schemes, including classical[37,38] and *ab initio* [based on the density functional theory (DFT)[38] and TDDFT[31,35,36]] molecular dynamics simulations have

been used to describe the effect of particle irradiation in carbon nanotubes and graphene. The classical molecular dynamics approach employs analytical potentials which allows simulations of large systems at low computational burden. The disadvantage of that approach is that analytic potential is only approximate and the quantum-mechanical nature of the process is neglected. Using quantum forces obtained from DFT calculations fixes some of the problems of the classical molecular dynamics approach at a price of higher computational demands. However, the DFT itself is a ground state theory. To describe the electronic excitations induced by the projectile, one must use TDDFT which gives a full dynamical description as we have described above. In the collision processes that we model in this work, the use of TDDFT is essential. Since the incident charged particle moves very rapidly (already at 3 keV, the proton has a velocity that is comparable to the Fermi-velocity of electrons in graphene) electronic excitations play a major role in the energy transfer and the dynamics of nuclei. The Born-Oppenheimer DFT molecular dynamics is not expected to provide an adequate description in such a regime.

In TDDFT[30] the time evolution of a system of interacting electrons is described by the time-dependent Kohn-Sham equation:

$$i\hbar\frac{\partial\psi_k(\mathbf{r},t)}{\partial t} = H\psi_k(\mathbf{r},t), \quad k = 1,\ldots,N. \tag{1}$$

Here, ψ_k are time-dependent single-particle Kohn-Sham orbitals and N is the number of occupied orbitals. The total electron density, which determines the properties of the system is defined as

$$\rho(\mathbf{r},t) = \sum_{k=1}^{N} f_k|\psi_k(\mathbf{r},t)|^2, \tag{2}$$

where f_k is the occupation number. The Kohn-Sham Hamiltonian H in Eq. (1) is a sum of the kinetic energy operator, the Hartree potential, the exchange-correlation potential, and the external potential:

$$H = -\frac{\hbar^2}{2m}\nabla_{\mathbf{r}}^2 + V_{\mathrm{H}}[\rho](\mathbf{r}) + V_{\mathrm{XC}}[\rho](\mathbf{r}) + V_{\mathrm{ext}}(\mathbf{r},t). \tag{3}$$

The external potential, in turn, consists of the contributions due to the ionic core and the time-dependent field created by a moving projectile. Hence

$$V_{\mathrm{ext}}(\mathbf{r},t) = V_{\mathrm{ion}}(\mathbf{r},\{\mathbf{R}(t)\}) + V_{\mathrm{proj}}(\mathbf{r},t). \tag{4}$$

Here, $\{\mathbf{R}(t)\}$ denotes the positions of all ions in the system, $\mathbf{R}_j(t)$, $j = 1,\ldots,N_{\mathrm{ions}}$. To represent the exchange-correlation potential V^{XC} we employed the adiabatic local density approximation (ALDA) with the parametrization by Perdew and Zunger.[39] The ionic core potential was taken as a sum of norm-conserving pseudopotentials by Troullier and Martins[40] centered at each ion. These pseudopotentials have both local and nonlocal components. The Hartree potential,

$$V_{\mathrm{H}}[\rho](\mathbf{r},t) = \int\frac{\rho(\mathbf{r}',t)}{|\mathbf{r}-\mathbf{r}'|}d\mathbf{r}' \tag{5}$$

was computed by numerically solving the Poisson equation. Lastly, the projectile potential was represented as a moving Coulomb potential,

$$V_{\mathrm{proj}}(\mathbf{r},t) = -\frac{\mathcal{Q}}{\sqrt{|\mathbf{r}-\boldsymbol{\mathcal{R}}(t)|^2+\epsilon^2}}, \tag{6}$$

where $\mathcal{Q}$ is the charge, $\boldsymbol{\mathcal{R}}(t)$ is the position of the particle, and ϵ is some very small parameter (softening radius) ensuring nonsingularity of the operator if it happens to be evaluated at an extremely short distance $|\mathbf{r}-\boldsymbol{\mathcal{R}}(t)|$. In our simulations, we set $\epsilon = 0.01$ Å.

In this work, we are primarily concerned with energetic charged particles (energy ranging from a few kilo-electron-volt to a few mega-electron-volt) colliding with graphene fragments. The energy change of the projectile due the interaction with the valence electrons of the single layer graphene is negligible, therefore we can assume that its trajectory is a straight line, $\boldsymbol{\mathcal{R}}(t) = \boldsymbol{\mathcal{R}}(0) + \boldsymbol{\mathcal{V}}t$, where $\boldsymbol{\mathcal{V}}$ is the projectile velocity.

The interaction with valence electrons is not the only energy transfer mechanism that can lead to creation of defects in the collision of energetic particles with graphene. A head-on collision of a charged particle with a carbon nucleus may provide sufficient amount of energy to create a defect by knocking an atom out. However, the probability of this event is small. The displacement of a carbon nucleus in a graphitic structure requires a transfer of at least 20 eV of energy.[15] A simple estimate based on a classical collision of two Coulomb particles (Rutherford scattering) suggests that for a 1 MeV proton to transfer 20 eV to a carbon nucleus requires an impact parameter of the order of $b \approx 0.005$ Å. This corresponds to a probability of less than 0.004% in a single layer graphene (assuming that the trajectory of incident protons is perpendicular to the graphene sheet). Even for a relatively slow 1 keV proton, the transfer of the same 20 eV to a carbon nucleus can occur when $b < 0.18$ Å (less than 4% probability). There is also a possibility for the projectile to interact with the inner-shell electrons. Due to the use of pseudopotentials, our simulations do not model such a process. Since the inner-shell electrons are deeply bound and localized around the nuclei it is reasonable to assume, however, that their role becomes important only when the projectile passes through a small region that surrounds the nuclei.

To represent the Kohn-Sham orbitals and the electron density we used real-space grids with uniform spacing of 0.25 Å along all three spatial coordinates. The graphene fragments (see Fig. 1) lie in the yz plane, while the projectile

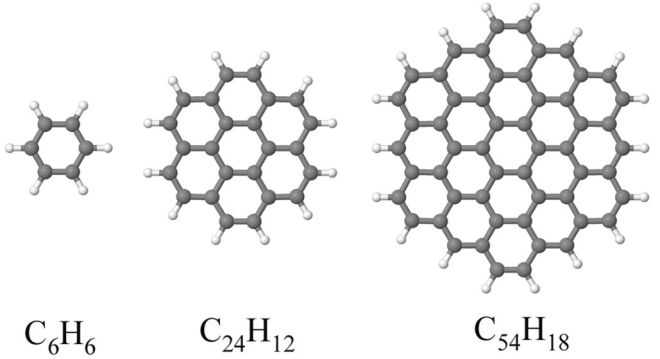

FIG. 1. Hydrogenated graphene fragments used in this work.

moves along the x axis. Our simulation cell is a rectangular box whose y and z boundaries were placed at a distance of approximately 5 Å from the closest atom. The boundaries in the x (projectile) direction are placed at a distance of 7.4–8.1 Å (depending on the particular graphene fragment) from the graphene plane. The kinetic energy operator in Eq. (3) was represented by a fourth-order finite difference approximation. It should be mentioned that due to the presence of the projectile the system is not periodic. We used free space boundary conditions for the Kohn-Sham orbitals.

Due to its flexibility, the real-space grid basis provides a more accurate description than atomic basis functions that are centered at ionic positions. This is especially true in the strong electric field of the charged projectile. For an adequate description of the process, one has to accurately represent the Kohn-Sham orbitals not only around the ionic centers but in the entire space around the graphene sheet. Another useful property of real-space numerical grids is the straightforward control of accuracy of the calculations. The accuracy can be increased or decreased by adjusting a single parameter, the grid spacing (just like the energy cutoff controls the accuracy in calculations employing plane-wave basis sets). Finally, the implementation of computational algorithms for explicitly time-dependent calculations is greatly simplified when real-space numerical grids are used.

Three graphene flakes of increasing size, C_6H_6, $C_{24}H_{12}$, $C_{54}H_{18}$ have been used in the calculations. Hydrogen atoms were added to the flakes to passivate the dangling bonds at the edges. Therefore, the smallest fragment consisting of a single carbon ring, is a benzene molecule, and the other two are known as coronene and circumcoronene. Their geometric structures are shown in Fig. 1.

Initially, i.e., before the collision with a projectile occurs, each system is in its ground state. The ground-state orbitals $\psi_k(\mathbf{r},0)$ are calculated by diagonalizing the time-independent Kohn-Sham Hamiltonian. At $t = 0$ fs, a charged particle was placed at a distance of 50 Å from the graphene fragment with an initial momentum corresponding to a given energy. Within $t = 0.3$–10 fs (depending on the particle energy) the projectile reached the graphene target. The total propagation time in the simulations was $T = 50$ fs. The Coulomb field of the projectile acts on the electrons during the whole simulation time both when the projectile is inside and outside of the simulation box. The fact that the initial and the final positions of the projectile is outside of the simulation box does not present a problem as long as the size of the simulation box is large enough to contain the electron charge density of the graphene and no charge transfer from the target to the projectile takes place. The charge transfer (see Fig. 2) may occur at very low projectile energies, when the electrons from the target system have enough time to "stick" to the charged particle. In our simulations, we have only observed significant charge transfer at very low projectile energies (1–5 keV).

The Kohn-Sham orbitals were propagated by a successive application of the short time time-evolution operator, $U(t,t+\Delta t) \approx \exp[-iH(t)\Delta t/\hbar]$ with a time step Δt. The total simulation time, $T = 50$ fs was divided into 50 000 time intervals, that is $\Delta t = 1$ attosecond is used in the calculations. A short time step is necessary to ensure that the time-dependent Hamiltonian remains nearly commutative at times t and

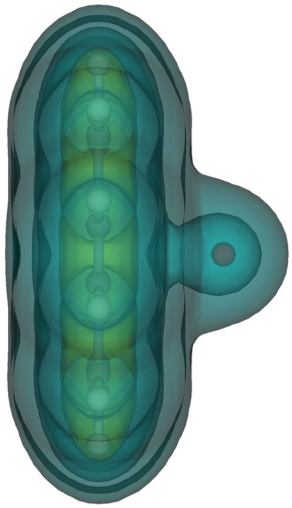

FIG. 2. (Color online) An illustration of the charge transfer to a slow projectile that just passed through a graphene fragment.

$t + \Delta t$ and the splitting of the total time-evolution operator $U(0,t_{\text{final}})$ into successively applied propagators remains valid. The smallness of the time step is also required for the stability of the Taylor-time propagation used in the calculations. The size of the time step that provides a stable time propagation usually decreases when the grid spacing is made smaller. To approximate the exponential form of the time-evolution operator, we used the fourth order Taylor expansion,

$$\exp\left[\frac{-iH(t)\Delta t}{\hbar}\right] \approx \sum_{n=1}^{4} \frac{\left[-\frac{iH(t)\Delta t}{\hbar}\right]^n}{n!}, \tag{7}$$

which, in our experience, provides a good balance between accuracy and computational cost.

The time propagation scheme outlined above allows one to model the time evolution of the electron density. As one of the main goals of this work is to study whether formation of defects is possible, that scheme has to be complemented with a set of equations that describe the motion of ions. In our simulations, the Ehrenfest approach is used to treat the dynamics of ions. In this approach, the ions move classically under the influence of the time-dependent quantum forces. The forces are calculated as the derivatives of the total energy with respect to the ionic positions. The corresponding equations of motion have the following form:

$$M_i \frac{d^2\mathbf{R}_i}{dt^2} = -\nabla_{\mathbf{R}_i}\left[\frac{\mathcal{Q}Z_i}{|\mathbf{R}_i - \boldsymbol{\mathcal{R}}|} + \sum_{j\neq i}^{N_{\text{ions}}} \frac{Z_i Z_j}{|\mathbf{R}_i - \mathbf{R}_j|} + \int V_{\text{ion}}(\mathbf{r},\mathbf{R}_i)\rho(\mathbf{r},t)d\mathbf{r}\right], \tag{8}$$

where M_i is the mass of the ith ion, and Z_i is its pseudocharge (valence). Equations (8) are coupled with the time-dependent Kohn-Sham equations (1) through the electron density, ρ. Equations (1) and (8) have to be solved simultaneously at each time step. To integrate equations (8), we used the Verlet algorithm. While in typical Born-Oppenheimer DFT molecular dynamics simulations the time step for the ionic motion can be chosen to be rather long (a fraction of the

smallest stretching period, i.e., hundreds of attoseconds), in our case, forces need to be evaluated at every (or nearly every) iteration of the electronic motion. This is because the electronic density can evolve quite rapidly, which may also cause fast variations of forces. In addition, we also have a fast moving Coulomb particle. In order to get an accurate net effect of its interaction with both the electron cloud and ions it is necessary to keep the integration step small.

Excessively steep potentials (even in those cases when the electronic density is small or vanishes in the vicinity of the points of "singularity") may cause inaccuracies or numerical instabilities in finite-difference calculations. One way of dealing with this problem would be to replace the actual Coulomb potential with its softened version [similarly to Eq. (6) but with a considerably larger ϵ] or with the hydrogen ion pseudopotential. In this work, however, in order to minimize the errors originating from the steepness of the Coulomb potential of the projectile, we selected the projectile's trajectory that lies approximately in the middle between the grid points. This choice helps to maintain the accuracy of calculations.

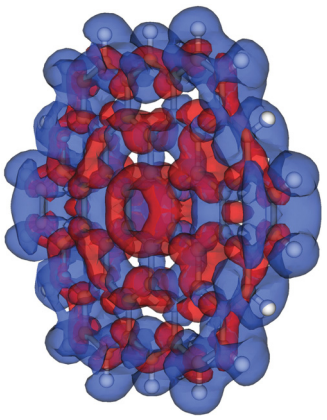

FIG. 4. (Color online) A snapshot of the density difference, $\rho(t) - \rho(0)$, taken soon after the projectile impact. For the case shown, the projectile energy was 300 keV and $t = 1.4$ fs. Red and blue areas indicate positive and negative values of the difference, respectively. For an animated version see Supplemental Material (Ref. 41).

III. RESULTS

In this work, we have mainly simulated a projectile impact through two points, namely, through the center of a carbon ring and through the middle of a carbon-carbon bond as shown in Fig. 3. From these two trajectories we estimate the expected variations in the energy transfer with respect to the impact geometry. The energies of the incident protons in the simulations are between 1 keV and 2 MeV. In terms of particle velocities this approximately corresponds to the range 4.4–196 Å/fs.

The qualitative picture of the collision process, which we model, is as follows. Upon the proton impact, the target system becomes polarized. Negatively charged electrons are pulled toward the positively charged proton when it passes through a graphene fragment. Immediately after the impact, the electron density starts oscillating, primarily in the radial direction. The oscillations quickly (within 0.2 fs) spread out and acquire a very complex pattern as shown in Fig. 4.

In the simulations, we have studied the ion dynamics during and after the collision and the transfer of energy from the projectile to the target. Monitoring the positions of individual ions allows us to track the creation of defects and changes in chemical bonding between atoms. Computing the difference between the final and initial energy of the target helps to elucidate the net effect of the electronic (and vibrational) excitations.

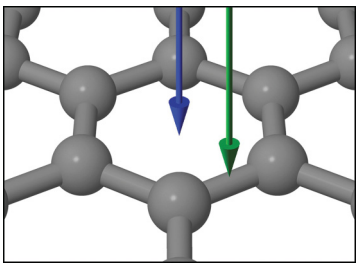

FIG. 3. (Color online) Two projectile trajectories systematically used in the present simulations: through a ring center and through a bond.

None of the simulations that involved a proton projectile have shown permanent changes in the geometric structures of the graphene fragments. This includes the smallest fragment, C_6H_6, which, due to its small number of atoms, is expected to be the easiest to break (since the transferred energy is eventually redistributed over the whole system). The largest amplitude of the ionic motion was observed for energy between 20 and 30 keV when the projectile hit the bond between carbon atoms. In that case, some of the ionic positions deviated from their equilibrium value by ≈0.2 Å.

The total energy transferred in the collision as a function of the proton impact energy for graphene fragments (C_6H_6, $C_{24}H_{12}$, and $C_{54}H_{18}$) is shown in Fig. 5. The plots show that more energy (0 to 40% in relative terms) is transferred to the target when the projectile passes through a C–C bond than when it does through the center of the carbon ring. This can be easily understood because the electron density is higher in the chemical bond region and the proton's interaction with the electrons is expected to be stronger. Going from the smaller system, C_6H_6, to the larger ones, $C_{24}H_{12}$ and $C_{54}H_{18}$, the amount of energy transferred somewhat increases. While the exact pattern of how and in what amount the energy is transferred depends on the electronic structure of the fragment, it is reasonable to assume that the general trend should be such that the larger the system the more energy is transferred. Upon increasing the size of the fragment the transferred energy should converge to the value corresponding to the infinite graphene sheet. It is interesting to note, however, that in our simulations the difference in the energy transfer is larger when going from $C_{24}H_{12}$ to $C_{54}H_{18}$ than from C_6H_6 to $C_{24}H_{12}$. While we cannot offer a simple explanation for this fact, one possible reason could be that in the case of C_6H_6 there are hydrogen atoms and they lie closer to the projectile trajectory than the carbon atoms in larger fragments (C–H

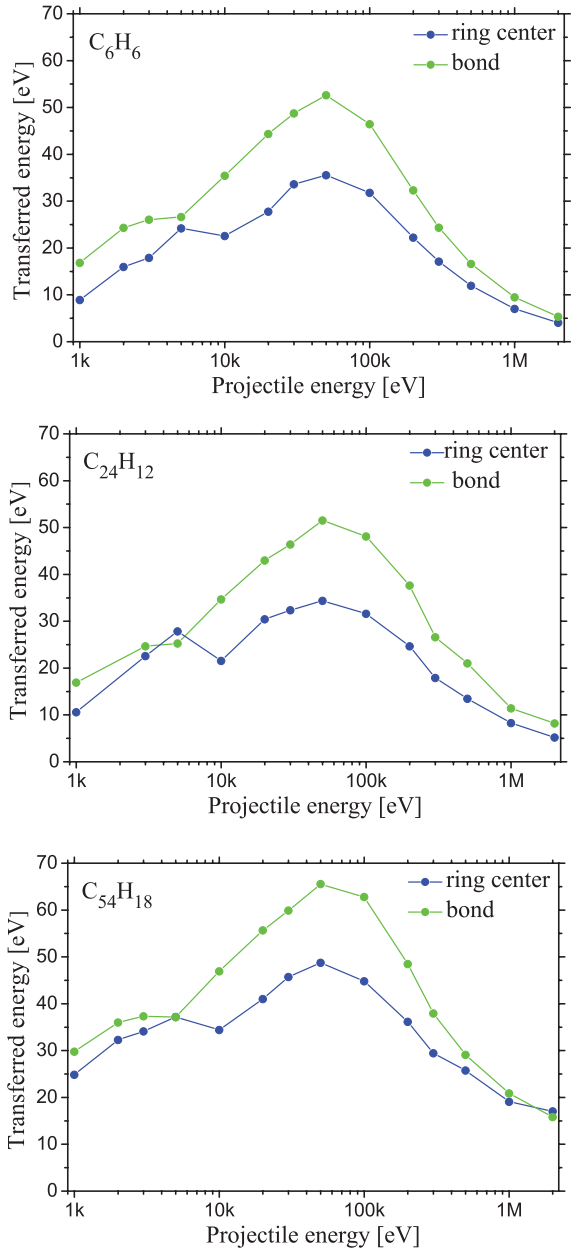

FIG. 5. (Color online) Total energy transferred to a graphene fragment as a function of proton energy.

bond in benzene is only 1.1 Å, while the C–C bond in graphene is 1.42 Å).

In absolute terms, the amount of energy transferred in a collision with a proton ranges from 5 to ∼52 eV for C_6H_6 and $C_{24}H_{12}$, and from 15 to ∼65 eV for $C_{54}H_{18}$ fragment. We estimate the accuracy of the calculated total transferred energies to be around 2–5 eV. The total transferred energy peaked at approximately 50 keV incident energy. While there is no experimental data for graphene, the measured proton stopping power in bulk graphite[42] peaks at ∼100 keV, which is in reasonable agreement with our calculations.

It should be noted that only a relatively small fraction of the total energy transferred (up to 0.1–3.0 eV, depending on the particular fragment and the impact point) appears to be in the form of vibrational excitations by the end of the simulations, at $t = 50$ fs. At no incident energies did we observe motion of nuclei that could lead to breaking of chemical bonds. The rest of the transferred energy, up to 65 eV, is accumulated as electronic excitations. In the real graphene, this energy would eventually be redistributed in the infinite sheet. Hence we can conclude that a high-energy proton passing through a single-layer graphene is unlikely to create any defects as a result of its interaction with valence electrons (as it was mentioned in the previous section a small probability of defect creation comes from nearly head on collisions with atomic nuclei).

In order to verify that the symmetry of the impact point locations (the center of a carbon ring and the middle of a C–C bond) does not result in some specific artifacts in the electronic and nuclear motion preventing creation of defects we have performed simulations with a proton passing through a C–C bond at a distance of 0.46 and 0.21 Å from the carbon ion (as opposed to 0.71 Å for the original impact point). These calculations have only been performed for the $C_{24}H_{12}$ fragment and the energy of the projectile was 50 keV. In addition to that, the calculations were repeated for both zero and 300 K initial temperature of the graphene fragment. We did not observe a dramatic change in the amount of transferred energy in any of the cases. Changing the impact parameter from 0.71 to 0.46 Å and then to 0.21 Å increased the energy fransfer from 51.5 to 55 and 59 eV, respectively. It must be emphasized, however, that due to the use of pseudopotentials the accuracy of TDDFT simulations deteriorates when the impact points gets closer to the ionic centers because the interaction with the core electrons is not taken into account. In the limit of very small impact parameter (the actual threshold value depends on the impact energy), the collision between the projectile and a carbon ion essentially becomes a classical collision of two Coulomb particles. To verify our implementation of molecular dynamics, we have simulated such a nearly head-on collision with a 20 keV proton and confirmed that the carbon ion gets easily kicked out of the system creating a single-atom vacancy.

Besides the incident energy, impact point, and particle's momentum direction, the outcome of collisions of energetic particles with molecules and solids is determined by another very important parameter—the charge of the particle. Highly charged particles and ions can perturb or damage the target system more significantly than protons or singly charged ions moving with the same velocity. In order to elucidate how increasing the charge of the projectile affects the electron and nuclear dynamics in graphene fragments, we carried out several simulations with α particles ($^4He^{2+}$). Based on the results of the calculation for protons, in the case of α particles we limited ourselves to the range of energies 30 keV–1 MeV (or 12–69 Å/fs in terms of particle velocity). As in the case of proton projectiles, the results for all three fragments were qualitatively similar. We only considered computationally less expensive cases of C_6H_6 and $C_{24}H_{12}$ when we performed simulations with α particles.

As expected, the interaction of α particles with the target systems was tangibly stronger and resulted in higher amounts of total energy transferred to the graphene fragments leading to larger kinetic energies of carbon and hydrogen ions. In fact, for the smallest fragment, C_6H_6, when we shot 50 and 100 keV α particles through the C–C bond, we observed a disintegration

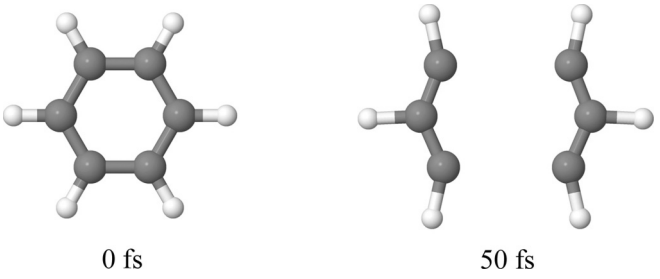

FIG. 6. The initial and final structures for C_6H_6 fragment when shot with a 50 keV α particle through a carbon-carbon bond.

of the target into two subsystems ($C_3H_3 + C_3H_3$) as shown in Fig. 6. At 30 and 300 keV incident energy disintegration did not occur within the 50 fs time interval, yet the amplitude of ionic motion was such that the target was almost broken. No disintegration was observed when an α particle with kinetic energy of 50 or 100 keV is passing through the center of C_6H_6. However, the amplitude of the radial (in the plane of the ring) oscillations was such that the distance between carbon ions reached 1.9 Å. In the larger fragment, $C_{24}H_{12}$, the motion of ions was considerably more restricted and no indication of immediate bond breakage was observed.

The plots of total energy transfer for the simulations that involved an α particle are shown in Fig. 7. The plots are given in the same scale as those for the simulations with a proton. One can notice an increased amount of the total energy transferred (up to approximately 150 eV) compared to the case of proton irradiation. The peaks are shifted to around 100–300 keV. This probably reflects the fact that the α particle is four times heavier than the proton and, hence, the same velocity corresponds to four times higher kinetic energy.

While in the present work we did not perform any simulations with more than doubly charged ions (such simulations are considerably more complex due to an unavoidable process of charge transfer from the target to the ion), based on the tendencies observed upon increasing the charge from $\mathcal{Q} = 1$ to 2, we speculate that irradiation of graphene with highly charged ions will probably break chemical bonds and create defects in graphene.

In summary, the coupled electron-ion dynamics is studied in small graphene fragments subjected to proton or α-particle irradiation with the energy of incident particles ranging from 1 keV to 2 MeV. The results show that the interaction between these particles and the valence electrons of carbon atoms in graphene is not strong enough to break chemical bonds.

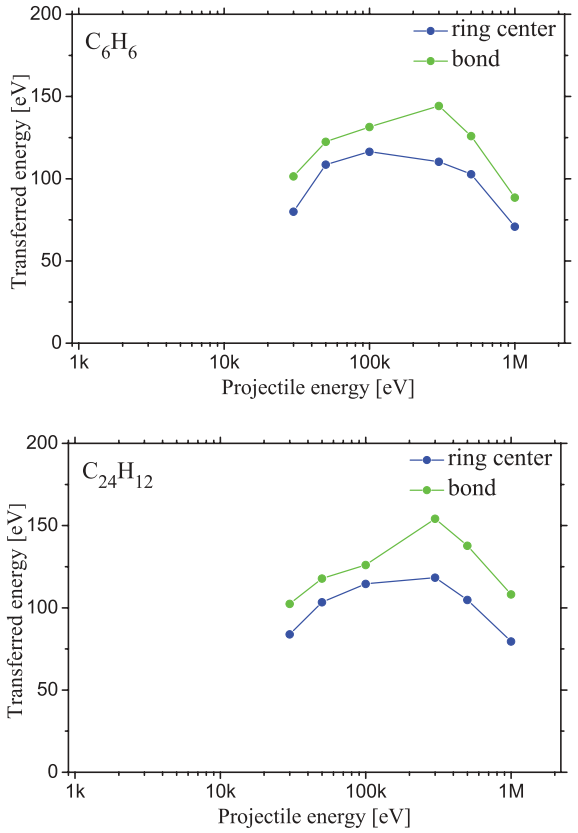

FIG. 7. (Color online) Total energy transferred in a collision with an α particle.

Therefore the mechanism of defect creation in graphene irradiated with protons and singly, or doubly charged ions must be entirely due to binary head-on collisions with carbon nuclei. We believe that the mechanism may be different when graphene is bombarded with highly charged ions. In that case, the ions may cause permanent damage in graphene even when their trajectories do not happen to lie in close proximity to a carbon nucleus.

ACKNOWLEDGMENTS

This work has been supported by the National Science Foundation (grant CMMI-0927345), Defense Threat Reduction Agency (grant HDTRA1-10-1-0016), Department of Energy (grant DE-FG02-09ER46554), and the McMinn Endowment at Vanderbilt University.

[1]K. S. Novoselov, A. K. Geim, S. V. Morozov, D. Jiang, Y. Zhang, S. V. Dubonos, I. V. Grigorieva, and A. A. Firsov, Science **306**, 666 (2004).
[2]A. K. Geim and K. S. Novoselov, Nat. Mater. **6**, 183 (2007).
[3]M. C. Lemme, D. C. Bell, J. R. Williams, L. A. Stern, B. W. H. Baugher, P. Jarillo-Herrero, and C. M. Marcus, ACS Nano **3**, 2674 (2009).
[4]B. Song, G. F. Schneider, Q. Xu, G. Pandraud, C. Dekker, and H. Zandbergen, Nano Lett. **11**, 2247 (2011).
[5]M. D. Fischbein and M. Drndić, Appl. Phys. Lett. **93**, 113107 (2008).
[6]D. C. Bell, M. C. Lemme, L. A. Stern, J. R. Williams, and C. M. Marcus, Nanotechnology **20**, 455301 (2009).
[7]S. Akcöltekin, H. Bukowska, T. Peters, O. Osmani, I. Monnet, I. Alzaher, B. B. d'Etat, H. Lebius, and M. Schleberger, Appl. Phys. Lett. **98**, 103103 (2011).
[8]J. F. Ziegler, J. P. Biersack, and U. Littmark, *The Stopping and Range of Ions in Matter* (Pergamon, New York, 1985).

[9]P. Sigmund, *Stopping of Heavy Ions: a Theoretical Approach*, Springer Tracts in Modern Physics (Springer-Verlag, Berlin and Heidelberg, 2004).
[10]M. A. Kumakhov and F. F. Komarov, *Energy Loss and Ion Ranges in Solids* (Gordon and Breach, New York, 1981).
[11]W. Eckstein, *Computer Simulation of Ion-Solid Interactions*, Springer Series in Materials Science (Springer-Verlag, Berlin, 1991).
[12]R. Smith, *Atomic and Ion Collisions in Solids and at Surfaces: Theory, Simulation and Applications* (Cambridge University Press, 1997).
[13]M. A. Nastasi, J. W. Mayer, and J. K. Hirvonen, *Ion-Solid Interactions: Fundamentals and Applications* (Cambridge University Press, 1996).
[14]P. Sigmund, *Particle Penetration and Radiation Effects: General Aspects and Stopping of Swift Point Charges* (Springer-Verlag, Berlin and Heidelberg, 2006).
[15]A. V. Krasheninnikov and F. Banhart, Nat. Mater. **6**, 723 (2007).
[16]F. Banhart, J. Kotakoski, and A. V. Krasheninnikov, ACS Nano **5**, 26 (2011).
[17]G. Ko, H.-Y. Kim, F. Ren, S. J. Pearton, and J. Kim, Electrochem. Solid-State Lett. **13**, K32 (2010).
[18]M. M. Ugeda, I. Brihuega, F. Guinea, and J. M. Gómez-Rodríguez, Phys. Rev. Lett. **104**, 096804 (2010).
[19]L. Tapasztó, G. Dobrik, P. Nemes-Incze, G. Vertesy, P. Lambin, and L. P. Biró, Phys. Rev. B **78**, 233407 (2008).
[20]E. Stolyarova, D. Stolyarov, K. Bolotin, S. Ryu, L. Liu, K. T. Rim, M. Klima, M. Hybertsen, I. Pogorelsky, I. Pavlishin, K. Kusche, J. Hone, P. Kim, H. L. Stormer, V. Yakimenko, and G. Flynn, Nano Lett. **9**, 332 (2009).
[21]G. Compagnini, F. Giannazzo, S. Sonde, V. Raineri, and E. Rimini, Carbon **47**, 3201 (2009).
[22]J.-H. Chen, L. Li, W. G. Cullen, E. D. Williams, and M. S. Fuhrer, Nat. Phys. **7**, 535 (2011).
[23]P. Esquinazi, D. Spemann, R. Höhne, A. Setzer, K.-H. Han, and T. Butz, Phys. Rev. Lett. **91**, 227201 (2003).
[24]P. O. Lehtinen, A. S. Foster, Y. Ma, A. V. Krasheninnikov, and R. M. Nieminen, Phys. Rev. Lett. **93**, 187202 (2004).
[25]J. Barzola-Quiquia, P. Esquinazi, M. Rothermel, D. Spemann, T. Butz, and N. García, Phys. Rev. B **76**, 161403 (2007).
[26]M. A. Ramos, J. Barzola-Quiquia, P. Esquinazi, A. Muñoz-Martin, A. Climent-Font, and M. García-Hernández, Phys. Rev. B **81**, 214404 (2010).
[27]T. L. Makarova, A. L. Shelankov, I. T. Serenkov, V. I. Sakharov, and D. W. Boukhvalov, Phys. Rev. B **83**, 085417 (2011).
[28]H. Ohldag, P. Esquinazi, E. Arenholz, D. Spemann, M. Rothermel, A. Setzer, and T. Butz, New J. Phys. **12**, 123012 (2010).
[29]S. Mathew, T. Chan, D. Zhan, K. Gopinadhan, A.-R. Barman, M. Breese, S. Dhar, Z. Shen, T. Venkatesan, and J. T. Thong, Carbon **49**, 1720 (2011).
[30]E. Runge and E. K. U. Gross, Phys. Rev. Lett. **52**, 997 (1984).
[31]A. V. Krasheninnikov, Y. Miyamoto, and D. Tománek, Phys. Rev. Lett. **99**, 016104 (2007).
[32]K. Yabana and G. F. Bertsch, Phys. Rev. B **54**, 4484 (1996).
[33]S. Bubin and K. Varga, Appl. Phys. Lett. **98**, 154101 (2011).
[34]S. Bubin and K. Varga, J. Appl. Phys. **110**, 064905 (2011).
[35]Y. Miyamoto, Appl. Phys. Lett. **91**, 113120 (2007).
[36]Y. Miyamoto and H. Zhang, Phys. Rev. B **77**, 161402 (2008).
[37]O. Lehtinen, J. Kotakoski, A. V. Krasheninnikov, and J. Keinonen, Nanotechnology **22**, 175306 (2011).
[38]O. Lehtinen, J. Kotakoski, A. V. Krasheninnikov, A. Tolvanen, K. Nordlund, and J. Keinonen, Phys. Rev. B **81**, 153401 (2010).
[39]J. P. Perdew and A. Zunger, Phys. Rev. B **23**, 5048 (1981).
[40]N. Troullier and J. L. Martins, Phys. Rev. B **43**, 1993 (1991).
[41]See Supplemental Material at http://link.aps.org/supplemental/10.1103/PhysRevB.85.235435 for animation of the electron dynamics in $C_{54}H_{18}$ graphene fragment during the collision with a 300 keV proton.
[42]M. J. Berger, J. S. Coursey, M. A. Zucker, and J. Chang, *Stopping-Power and Range Tables for Electrons, Protons, and Helium Ions (NIST Standard Reference Database 124)* (2005), available online at [http://www.nist.gov/pml/data/star/].